AIAA 80-0174R

Experimental Investigation of the Asymmetric Body Vortex Wake

William L. Oberkampf*
University of Texas at Austin, Austin, Texas
F. Kevin Owen†
Complere, Inc., Palo Alto, Calif.
and
T. P. Shivananda‡
University of Texas at Austin, Austin, Texas

An experimental investigation of the asymmetric body vortex wake of a circular cylinder in high subsonic flow is presented. Laser velocimeter, force and moment, and surface hot wire measurements were obtained for a freestream Mach number of 0.6 and Reynolds number (based on body diameter) of 0.62×10^6. Two component laser velocimeter measurements were made at three body cross-flow planes and three angles of attack. Laser vapor screen photographs were also obtained which show detailed structure of the wake flow. Surface hot wire measurements were used to determine if any vortex switching occurred at various angles of attack of the body. Laser velocimeter measurements are discussed in relation to the vapor screen photographs and side force measurements. These results show that, for the test Reynolds number, more than one asymmetric body vortex wake configuration can exist for the same angle of attack and body roll angle.

Nomenclature

d	= body diameter
C_y	= side force coefficient, $F_y/q_\infty S_b$
M_∞	= freestream Mach number
q_∞	= freestream dynamic pressure
R_d	= Reynolds number based on diameter, $U_\infty d/\nu$
S_b	= cross-sectional area of body, $\pi d^2/4$
U_∞	= freestream speed
u,v,w	= velocity components in the body coordinate system (see Fig. 3)
u',v',w'	= velocity components in the wind tunnel coordinate system
x,y,z	= body coordinate system (see Fig. 3)
α	= angle of attack of the body
ν	= kinematic viscosity

I. Introduction

THE importance of high angle of attack aerodynamics with regard to aircraft and missile flight is well recognized. If the angle of attack of a slender body of revolution is larger than roughly 25 deg, the symmetric body vortex wake breaks down and becomes asymmetric. The presence of the asymmetric vortex wake is known to produce large, destabilizing side forces and yawing moments. If aft mounted lifting surfaces are located in the asymmetric wake, then the stability and control problems are greatly complicated. Unfortunately, the precise mechanics through which these forces and moments occur are not sufficiently understood to enable reliable prediction. Until recently much of the research on asymmetric vortex flows has been restricted to force and moment measurements and to attempts to solve problems associated with particular design geometries. With detailed surface and flowfield measurements, however, mathematical models of the wake flow could be improved, thereby aiding in aircraft and missile design for very high maneuverability.

Experiments during the last several years have shown the extreme sensitivity of the asymmetric vortex flow. For example, visual studies have shown that minute imperfections on the model nosetip can determine whether the vortices are shed as left first, then right, or vice versa. Rotation of the body through just a few degrees in roll can cause the vortices to adjust from one system to another, thus changing forces and moments on the body.[1,2] Because of this sensitivity, nonintrusive velocity measurement techniques are considered the most reliable. Laser velocimeter measurements of the incompressible asymmetric wake were conducted by Fidler et al.[3] and Yanta and Wardlaw.[4] The first LV measurements of the body vortex wake in transonic flow were made by Owen and Johnson.[5] Until the present work, however, no measurements have been made of the compressible vortex wake in a large scale wind tunnel.

The present paper describes an experimental investigation of the asymmetric body vortex wake of a circular cylinder in high subsonic flow. Laser velocimeter, force and moment, and surface hot wire measurements were obtained for a freestream Mach number of 0.6 and Reynolds number (based on body diameter) of 0.62×10^6. Two component laser velocimeter measurements were made at three body cross-flow planes, $x/d = 4$, 8, and 12, and angles of attack, 25, 35, and 45 deg. Laser vapor screen photographs were also obtained at these body stations and angles of attack. Surface hot wire measurements were used to determine if any vortex switching occurred at various angles of attack of the body. LV measurements were obtained with the measurement plane at two different orientations with respect to the body but, because of changes in the flowfield, the measurements could not be combined in order to determine all three velocity components. Results of the LV measurements are related to the laser vapor screen photographs and side force measurements. A detailed explanation is given concerning the interpretation of the vapor screen photographs.

Presented as Paper 80-0174 at the AIAA 18th Aerospace Sciences Meeting, Pasadena, Calif., Jan. 14-16, 1980; submitted March 7, 1980; revision received March 16, 1981.

*Associate Professor, Dept. of Mechanical Engineering; presently with Sandia National Laboratories, Albuquerque, N. Mex. Associate Fellow AIAA.

†Consultant. Member AIAA.

‡Research Associate, Dept. of Mechanical Engineering; presently with TRW Systems and Energy, Redondo Beach, Calif. Member AIAA.

II. Instrumentation and Experimental Procedure

A. Wind Tunnel and Model

The experiment was conducted in the 1.83 m × 1.83 m (6 ft × 6 ft) wind tunnel of the NASA Ames Research Center. The tunnel is a continuous flow, closed-circuit wind tunnel with a test section incorporating a perforated floor and ceiling. The Mach number in the test section can be continuously varied from 0.25 to 2.2 by means of an asymmetric sliding block nozzle. The Reynolds number can be varied from 3.3×10^6/m (1.0×10^6/ft) to 16.4×10^6/m (5.0×10^6/ft).

The model was a 76.2 mm (3 in.) diam circular cylinder with a two caliber tangent ogive nose. The length of the complete body (nose and afterbody) was 1.143 m (45 in.) yielding a length-to-diameter ratio of 15. The model surface was polished to a finish of approximately 4 microinches and extreme care was taken to protect the nosetip before and during the experiment. The model was supported by a sting and 45 deg offset strut assembly attached to the main model support system (Fig. 1).

B. Strain Gage and Surface Wire Instrumentation

A Task Corp. strain gage balance was installed inside the model. The signal from the gages was input to the Indicating Millivolt Potentiometer System (IMPS) and a magnetic tape recorder. The IMPS contains servo-driven mechanical display dials which indicate the raw data signal. The IMPS essentially filters all signals above about 2 Hz. The analog output from the IMPS was sampled by a Beckman data acquisition system, digitized, and transmitted to the local IBM 360/67 computer. Three samples of a given channel were averaged in the data processing done on the IBM 360 in order to form a single output measurement. The time delay between each sample was 1.2 s.

The model was instrumented with two constant temperature surface hot wire gages. Both gages were located at $x/d = 13$ with a separation of 180 deg in roll angle. The output from the wires was recorded on a magnetic tape recorder for various roll angles and angles of attack of the body. Their dynamic response (greater than 60 KHz with negligible phase distortation[6]) was sufficient to determine the dynamic characteristics of the wake.

C. Laser Velocimeter Instrumentation

The velocity in the wake of the body was measured with a two-color, forward scatter, frequency offset laser velocimeter which enabled the simultaneous measurement of two independent velocity components. A schematic of the transmitting optics of the LV is shown in Fig. 2. With this system, the two primary laser lines, namely 0.4880 and 0.5145 μm, were separated by means of a prism, P. These primary beams were each split by the Bragg cells B_1 and B_2 to obtain two pairs of divergent, frequency-offset beams. Each pair of beams then passed through a "cube" (C_1 and C_2) that was ground to be slightly off-square to rectify the divergence. The four resultant parallel beams proceeded through the sending optics and were focused at the same point within the flow test region. Collecting optics on the far side of the wind-tunnel test section refocused the scattered light onto a pair of photomultiplier tubes. The signals from these tubes were then processed to obtain two components of velocity of particles passing through the focal volume. Figure 1 shows the transmitting optics used during the experiment.

The Bragg cells, which produce zero-velocity frequency offsets in both color systems, were incorporated to remove directional ambiguity from the measurements. If this element of the instrumentation is not included in the optics, then measurements made in flows that possess a high degree of turbulence or contain velocity direction reversals are suspect. Both the sending and collecting optics were mounted on a three-dimensional traverse system which moved in tandem

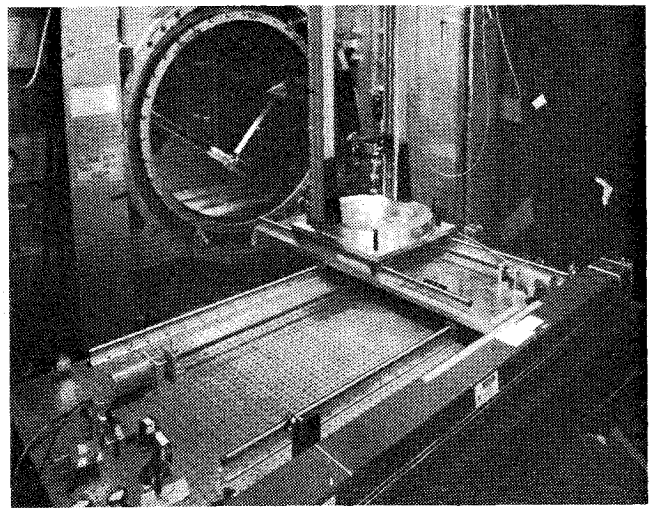

Fig. 1 Wind tunnel installation.

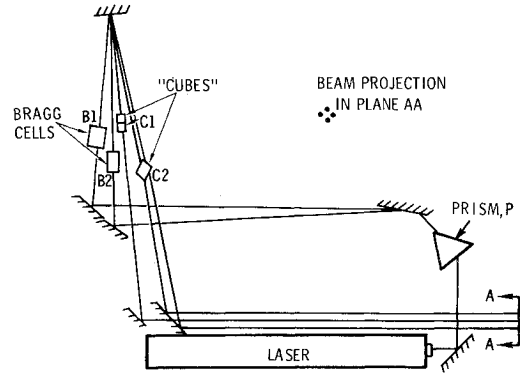

Fig. 2 Schematic of laser velocimeter sending optics.

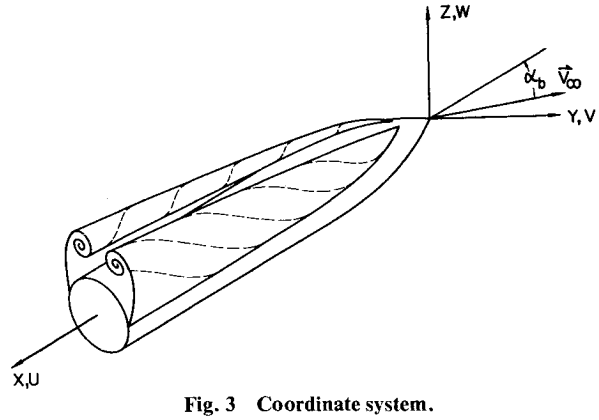

Fig. 3 Coordinate system.

(Fig. 1). The traverse system encoders were controlled by an HP 9825 calculator. Although the forward scatter system provided data rates in excess of 1000 samples/s, the alignment problems with a system this large should not be ignored. Because of the high data rates achieved with naturally occurring submicron particles, seeding was not used during the flowfield measurements.

As three velocity components were desired, two sets of LV measurements were taken. In the first set, the laser beams were set normal to the tunnel axis so that the wind tunnel axial (u') and vertical (w') velocity components were found. From these two components the body axial (u) and vertical (w) velocities in the cross-flow plane perpendicular to the body axis could be resolved. Figure 3 shows the body coordinate system. For the second set of measurements, the transmitting optics were rotated 21 deg about the z' axis and the

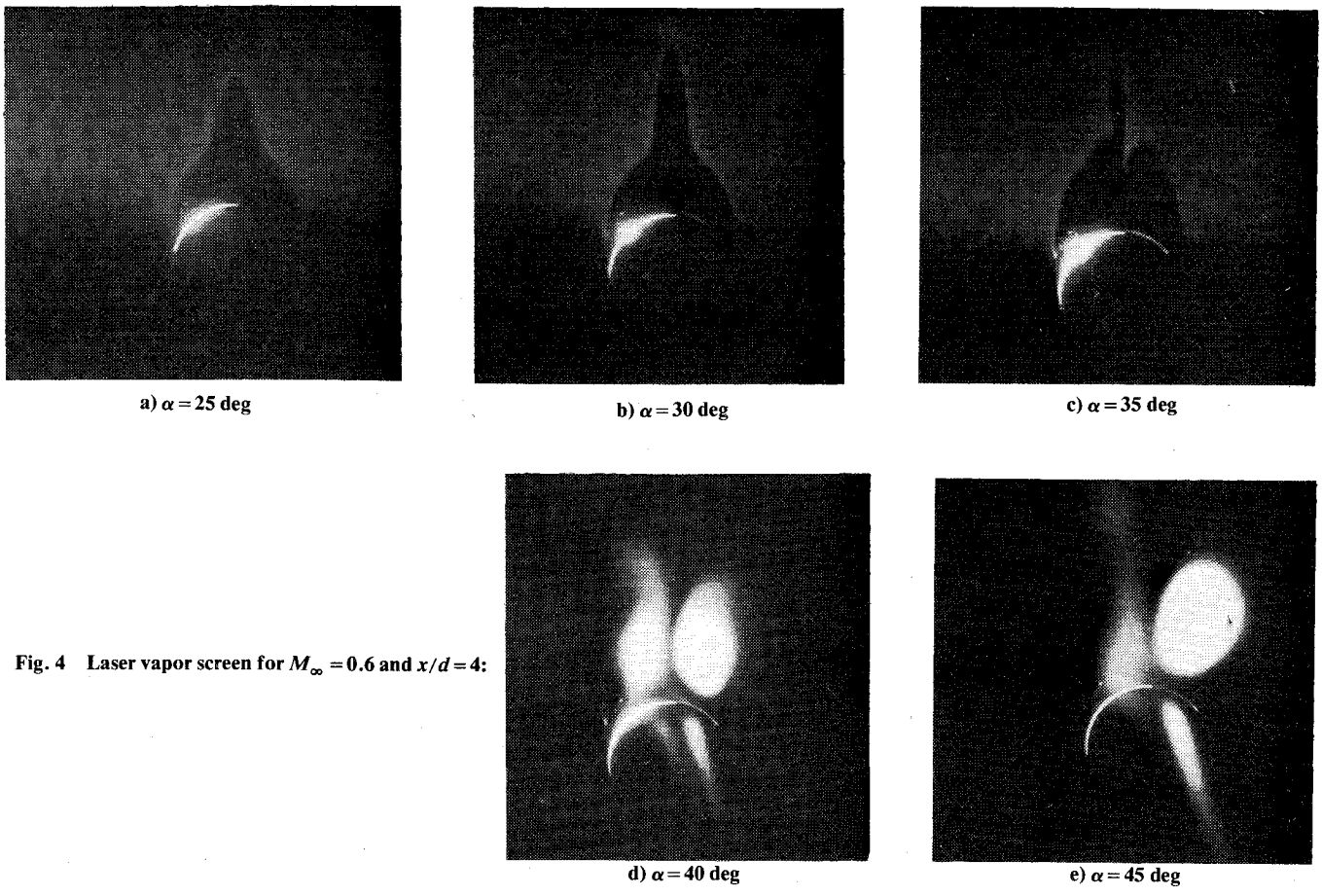

a) $\alpha = 25$ deg b) $\alpha = 30$ deg c) $\alpha = 35$ deg

d) $\alpha = 40$ deg e) $\alpha = 45$ deg

Fig. 4 Laser vapor screen for $M_\infty = 0.6$ and $x/d = 4$:

measurements repeated. Now, one velocity component measured was again the wind tunnel vertical velocity, whereas the second was a combination of the wind tunnel axial velocity (u') and lateral velocity (v'). As the axial velocity had already been measured, the lateral velocity could then be calculated, assuming the flowfield is the same.

A slight modification of the sending optics provided a valuable flow visualization tool: a laser vapor screen. This modification enabled either the 0.4880 or the 0.5145 μm lines to pass through a plane/cylindrical lens system so that a sheet of laser light could be generated to illuminate the cross-flow plane. By changing the location of the beam focus, a sheet of variable thickness and divergence angle could be produced. The lens could be rotated manually about the y axis and longitudinally and vertically using the velocimeter traverse gear such that any cross-sectional plane in the flow within the field of view circumscribed by the tunnel window could be observed. This traversing flexibility and very thin focused light sheet has enabled superior vortex flow visualization compared with previous mercury vapor light sources. Photographs of the scattered light were taken with a camera mounted on the strut support. In addition to providing detailed flow visualization, this technique provides a convenient means to determine suitable areas for detailed laser velocimeter measurements.

III. Results and Discussion

A. Vapor Screen Photographs

A large number of vapor screen photographs were taken during the course of the experiment. As mentioned in Sec. IIC, the sheet of light needed for the vapor screen was produced by placing a final cylindrical lens in the path of the laser so that the beam was spread in a plane perpendicular to the model axis. The camera was mounted on the left side (looking upstream) of the model support strut. The 45 deg support strut can be seen in Fig. 1 but the camera had been removed at the time the installation photograph was taken. The photographic axis was parallel to the model axis although it was slightly to the left and above the model, looking upstream.

Figure 4 shows a sequence of vapor screen photographs for $M_\infty = 0.6$ for $\alpha = 25$, 30, 35, 40, 45 deg at $x/d = 4$. The reflection of the laser on the left side of the body, the sheet of light being projected from left to right, and the shadow of the body on the right can be seen in the photographs. The body vortex wake flow is suggested in the dark regions of Figs. 4a-c and the light regions of Figs. 4d and 4e. As this angle of attack sequence of dark and light body vortices suggests, the interpretation of vapor screen photographs is not intuitive. An explanation will be given, however, which attempts to qualitatively interpret the present vapor screen photographs.

Vapor screen photographs image the condensation/evaporation of a gas/liquid mixture in a flowfield where there are large spatial changes in static pressure, temperature, and density. The interpretation of vapor screen photographs is also complicated by the fact that the two phase liquid/vapor mixture probably does not achieve thermodynamic equilibrium in the time a particle passes through the temperature, pressure, density field produced by the body. In preparing the wind tunnel airstream for the vapor screen flow visualization, steam is added to the tunnel until some type of wake flow can be seen near the model. For $x/d = 4$ and $\alpha = 25$-35 deg (Figs. 4a-c) this requires that enough water vapor be added to the tunnel so that the freestream flow passes from the superheated vapor phase to a liquid/vapor mixture, i.e., condensation has occurred for the given p_∞, T_∞. The reflection of light from the liquid droplets in the vapor can be seen above and to the side of the body (Figs. 4a-c). For $\alpha = 40$ and 45 deg (Figs. 4d and 4e), however, less water vapor need be added to the tunnel because a large amount of condensation occurs in the body wake first, that is, before it does in the freestream.

The dark wake flow region for $\alpha = 25$, 30, and 35 deg (Figs. 4a-c) reveals the locations where the freestream condensate has evaporated, thereby passing back into the superheated vapor phase. From this it can be concluded that the spatial boundary between the dark and light regions in the wake corresponds to the thermodynamic boundary of the saturated vapor. The reason for the water passing into the vapor phase in the wake is the increase in local static temperature. The fluid in and around the body vortices originated from the body boundary layer. In this shear layer the static temperature increases nearly to the total temperature. Although the static pressure drops in the body vortices, the increase in static temperature dominates thereby causing the liquid/vapor mixture (freestream) to pass into the pure vapor phase. From this explanation two conclusions can be drawn concerning the wake region without condensate. First, the dark region of the wake flow does not precisely represent the body vortices. The body vortices lie inside the dark region near the body and are not related to the temperature plume emanating from the top of this region. Second, the boundary between the dark and light regions is not a cross-flow plane dividing streamline. The boundary is the locus of points such that the locally elevated temperature from the body boundary layer balances with the local static pressure to yield a saturated vapor.

For angles of attack of 40 and 45 deg (Figs. 4d and 4e) the visualization of the body vortices has reversed as compared to $\alpha = 25$, 30, and 35 deg. For the higher angles of attack the body vortex strength has increased to the point where the low static pressure dominates over the increase in static temperature, thereby producing significant condensation. As the vortex strength increases, the local total pressure decreases. Even though there is a slight decrease in local Mach number, which tends to increase the static pressure for a constant total pressure, the large loss in total pressure causes the static pressure to decrease.§ From this explanation it can be concluded that the right body vortex for $\alpha = 40$ deg (Fig. 4d) is slightly stronger than the left vortex because of the larger region of condensate formed. For $\alpha = 45$ deg (Fig. 4e) the right vortex is still a strong, well organized vortex while the left vortex has dissipated substantially. The left vortex has lost sufficient concentrated vorticity so that the pressure is not low enough to condense water. This is not to say, however, that the total strength of the left vortex at $\alpha = 45$ deg is less than that at $\alpha = 40$ deg.

Vapor screen photographs for $M_\infty = 0.6$ at $x/d = 8$ and $\alpha = 25$, 35, and 45 deg are given in Fig. 5. An overlay nondimensional scale is given in Fig. 5 in order to correlate the photographs with the laser velocimeter measurements discussed in Sec. IIIC. The laser vapor screen photographs were printed such that the dimensional scale shown in Fig. 5 also applies to all vapor screen photographs given in the paper. For $\alpha = 25$ deg (Fig. 5a) the equal size regions of superheated vapor on each half-plane of the wake imply that the body vortices are still symmetric. For $\alpha = 35$ deg (Fig. 5b) the wake is clearly asymmetric. As seen for $x/d = 4$ and $\alpha = 45$ deg (Fig. 4e), the right vortex has sufficient strength to condense the vapor while the left vortex does not have sufficient localized vorticity to condense any vapor. For $\alpha = 45$ deg (Fig. 5c) the development of the wake into a von Kármán vortex street is clearly displayed. A vortex can be seen in the upper right portion of the wake, then a strong vortex lower on the left, and then a newly formed vortex on the lower right near the body.

§To corroborate this explanation of the balance between local static pressure and temperature, several photographs were obtained for $M_\infty = 0.7$ in which the body vortices are primarily dark, i.e., temperature dominating pressure, except for a small region of condensate in the middle of the superheated vapor region. This is because the lowest static pressure in the vortex is precisely in the center of the vortex.

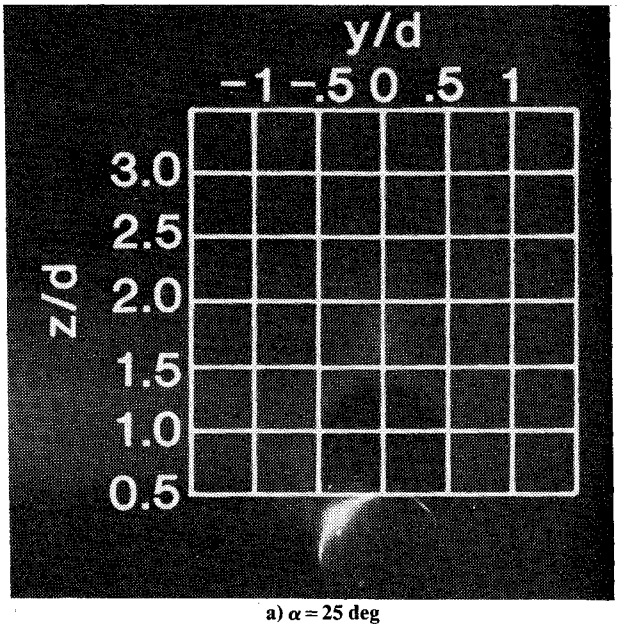

a) $\alpha = 25$ deg

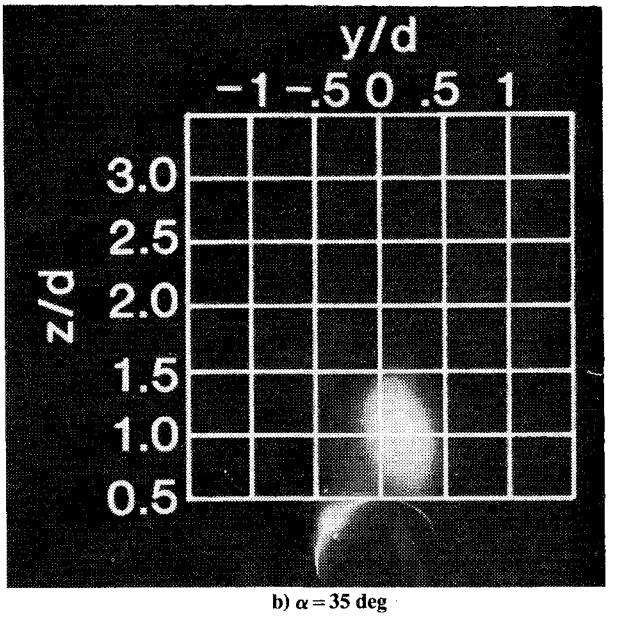

b) $\alpha = 35$ deg

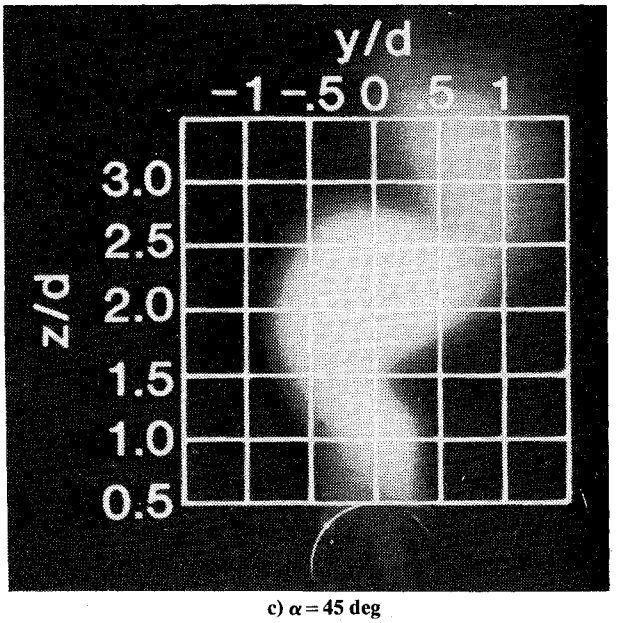

c) $\alpha = 45$ deg

Fig. 5 Laser vapor screen for $M_\infty = 0.6$ and $x/d = 8$.

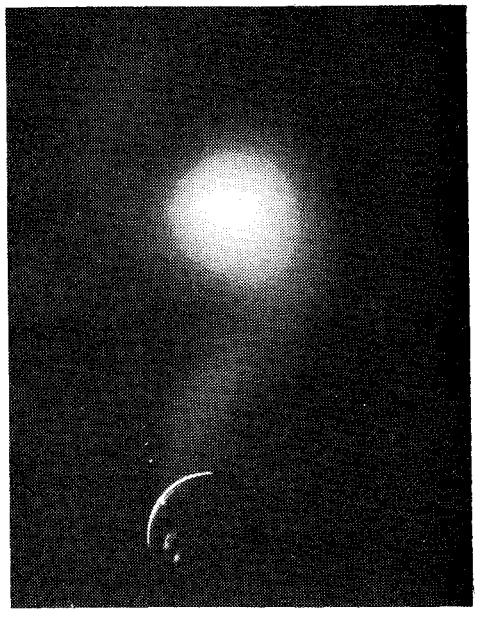

a) $\alpha = 35$ deg

b) $\alpha = 45$ deg

Fig. 6 Laser vapor screen for $M_\infty = 0.6$ and $x/d = 12$.

The vortex wake for $M_\infty = 0.6$ at $x/d = 12$ for $\alpha = 35$ and 45 deg can be seen in Fig. 6. For $\alpha = 35$ deg (Fig. 6a) only one strong vortex can be seen high above the surface of the body. As discussed earlier, this does not imply it is the only vortex in the wake, but only that it is the only one sufficiently concentrated to condense water vapor. For $\alpha = 45$ deg (Fig. 6b) the height of the vortex street is so large that it goes off the frame of the photograph. All of the multiple shed vortices are diffused to the extent that only a sparse trial of condensate marks their locations.

B. Surface Hot Wire and Force Measurements

Although the model could not be continuously rolled, surface hot wire signals were recorded for three different roll angles during one portion of the experiment. These roll positions were alternately chosen so that the gages were in the attached boundary layer, in the region of separation, and far past separation. Autocorrelations and power spectral densities were obtained in these regions. Power spectral densities,

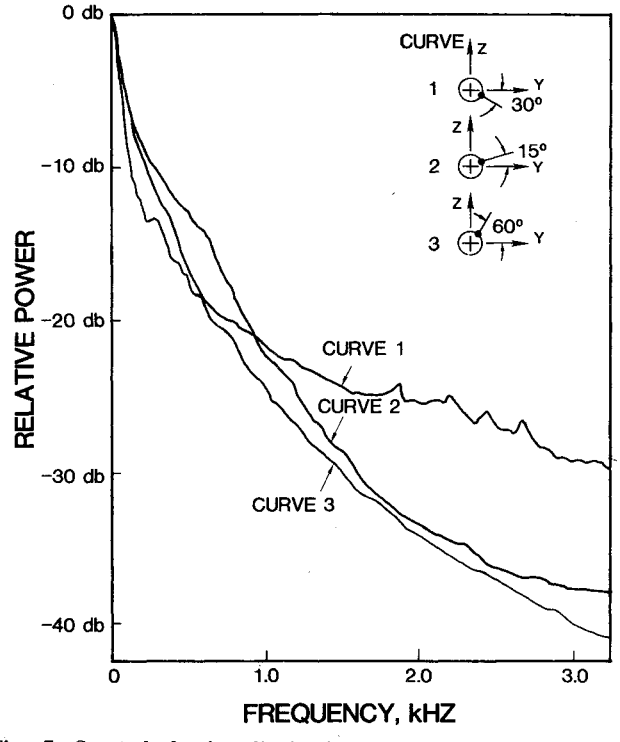

Fig. 7 Spectral density distribution for surface hot wire for $M_\infty = 0.6$, $\alpha = 45$ deg, and $x/d = 13$.

obtained by real time analysis of the hot wire signals, are shown in Fig. 7. Ahead of separation there is substantial high frequency (small turbulent scale) content typical of turbulent boundary layers (curve 1). In regions of separation and recirculation this high frequency content is dominated by large scale motions. However, of significance is the fact that no periodic signal content was observed in either the autocorrelations or the real time spectra. This supports the evidence that there was no unsteady vortex motion or mirror switching of the vortices on the time scale of seconds or less. Although hot wire measurements indicate relatively high freestream turbulence (0.6%), the integral time scales correspond to several body lengths. Such large scale fluctuations would not be expected to drive vortex unsteadiness.

The side force is known to be very sensitive to many factors, such as minute imperfections on the model nose, roll angle, and wind tunnel turbulence.[1,2,7,8] With this in mind, great care was taken to try and insure repeatability of the measurements. The nosetip was physically protected before the experiment and any time personnel were inside the tunnel. Also, the model roll angle was not changed at any time during the acquisition of force and moment or LV data. Because of the care taken with the model and the fixed roll angle, it was believed that the forces and moments on the body should be the same for the same angle of attack and Mach number. Late in the experiment, however, it was discovered that the side force and yaw moment were not always repeatable from one day to the next. Figures 8 and 9 show the magnitude of the side force coefficient vs run number for $M_\infty = 0.6$ for $\alpha = 35$ and 45 deg, respectively. The number of times a given value of side force was repeatedly measured for the same run number is indicated by the partial or total shading of the data symbol. Strain gage balance readings were recorded about every 15 min during tunnel operation. Typically three run numbers were executed during one 8-hr shift day. The data shown in Figs. 8 and 9 were obtained over a three-week period.

In order to eliminate any data which would be suspect because of high water vapor content in the tunnel, all of the vapor screen runs have been deleted (run nos. < 32). For run nos. ≥ 32 the tunnel was evacuated and filled with dry air at the beginning of each shift to ensure low water vapor content.

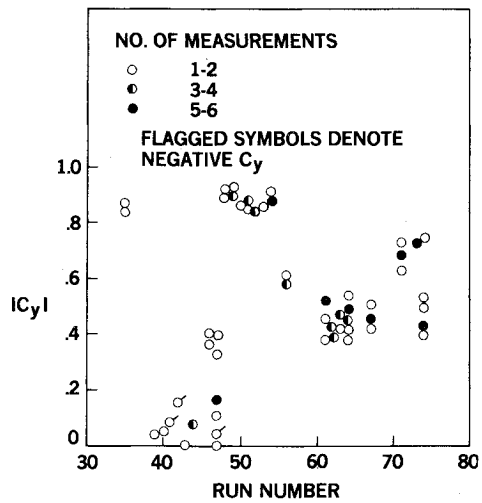

Fig. 8 Magnitude of side force coefficient vs run number for $M_\infty = 0.6$ and $\alpha = 35$ deg.

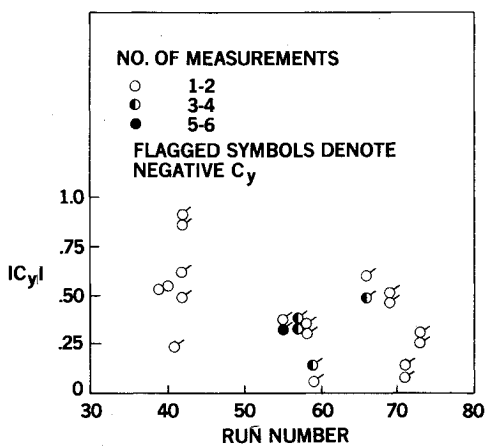

Fig. 9 Magnitude of side force coefficient vs run number for $M_\infty = 0.6$ and $\alpha = 45$ deg.

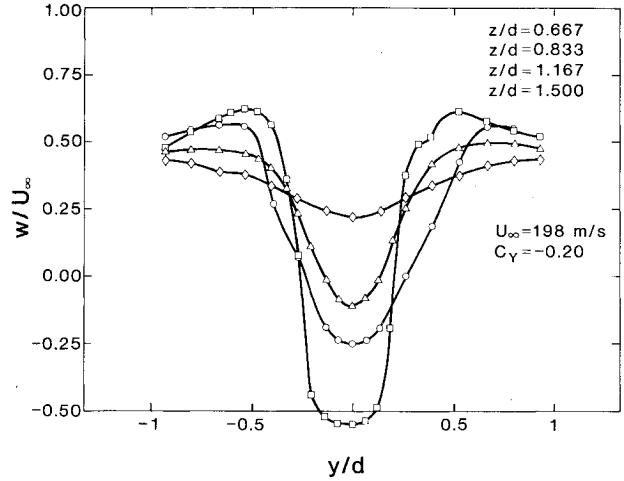

a) w/U_∞ vs y/d

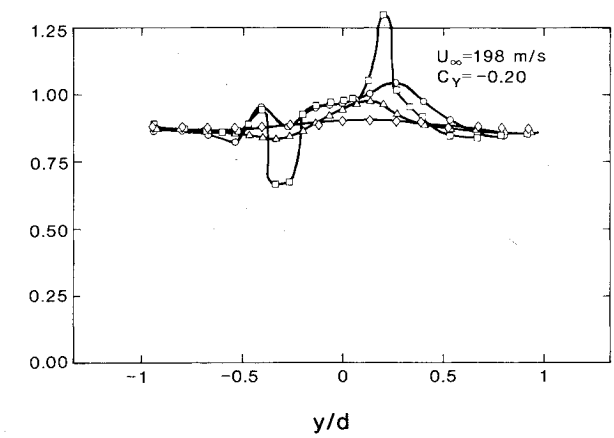

b) u/U_∞ vs y/d

Fig. 10 Laser velocimeter measurements for $M_\infty = 0.6$, $\alpha = 25$ deg, and $x/d = 8$.

Also, to eliminate any suspect data because of slight flowfield variations whose period was on the order of seconds, these data have been deleted. This was done by examining the three individual raw data readings which are used to calculate the final average value. Data whose variation between the largest and smallest of the three raw data readings was larger than 0.1 (in dimensionless coefficient form) were deleted from the final data set. This stringent criterion eliminated about 30% of the force and moment data. The data shown in Figs. 8 and 9 have been processed in the described manner.

Even though the previously described procedures were used to insure side force repeatability, the data of Figs. 8 and 9 show extremely large variations in side force. These variations, however, occur from one run or set of runs to the next with only a few exceptions. The side force data are generally grouped at certain values of side force for a given angle of attack. For example, at $\alpha = 35$ deg there is a large amount of data at side force values of 0.1, 0.4, 0.7, and 0.9. In order to generate these large, repeatable variations in side force the asymmetric body vortex wake must be able to exist in multiple metastable states. That is, clearly different side force values and the associated asymmetric wake could be repeated days and weeks apart. The exact nature of these multiple states, however, could not be determined from the LV data obtained in the experiment. Other experimenters in the past may have observed this same phenomenon but because of the lack of sufficient repeat runs, over a period of weeks, they discarded the data.

It should be pointed out that multiple vortex states for the same roll angle may not exist for other Reynolds numbers. The Reynolds number based on cross-flow velocity suggests that flow separation is in the transitional range; 0.36×10^6, and 0.44×10^6 for $\alpha = 35$ and 45 deg, respectively. The Reynolds number used by Lamont and Hunt[7] ($U_\infty d \cos\alpha/\nu$), however, suggests that separation is turbulent; 1.08×10^6, and 0.88×10^6 for $\alpha = 35$ and 45 deg, respectively. The surface hot wire signal also indicates that the boundary layer was turbulent before separation.

C. Laser Velocimeter Measurements

Two sets of laser velocimeter measurements were obtained during the experiment; (u', w') for the beams perpendicular to the tunnel axis, and $(V(u', v'), w')$ for the beams 21 deg from the normal to the tunnel axis. The two independent measurements for w' at the same location and conditions did not agree because the vortex fields were different. This is corroborated by noting the difference in the side force coefficients between the various runs discussed earlier. For example, the LV measurements for the beams perpendicular to the tunnel for $\alpha = 35$ deg were conducted primarily during runs 48-54. Referring to Fig. 8, it is seen that the side force was always near 0.9. The LV measurements for the beams 21 deg off normal were conducted during runs 61-64. For the latter runs the side force coefficient was near 0.4. Because of this difficulty, only LV measurements obtained perpendicular to the tunnel axis will be presented.

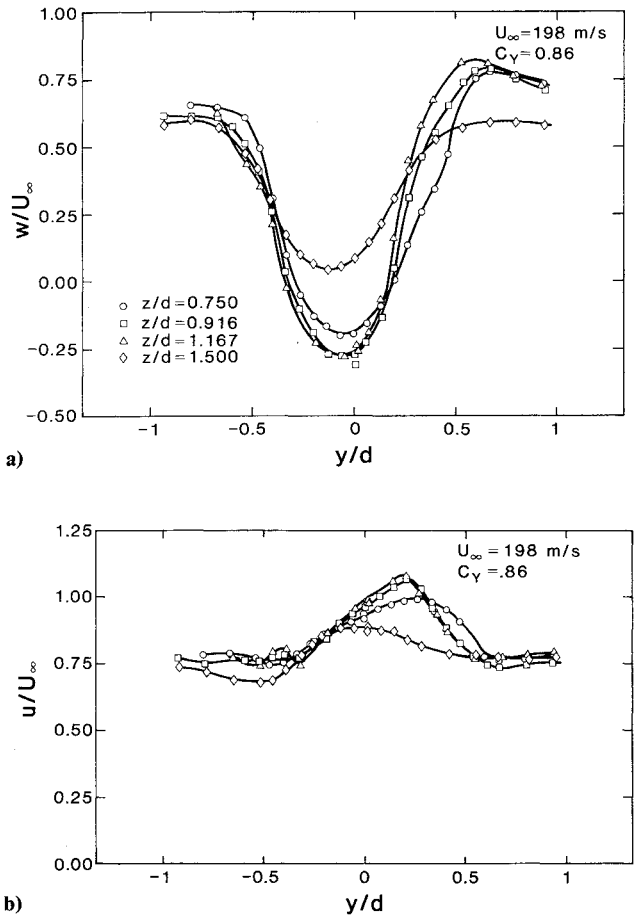

Fig. 11 Laser velocimeter measurements for $M_\infty = 0.6$: $\alpha = 35$ deg, and $x/d = 8$; a) w/U_∞ vs y/d; b) u/U_∞ vs y/d.

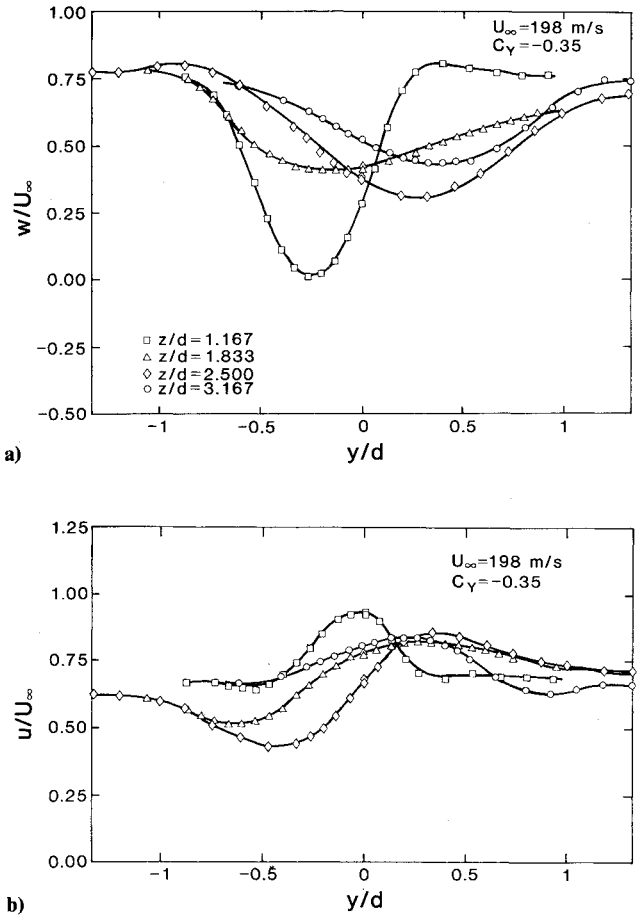

Fig. 12 Laser velocimeter measurements for $M_\infty = 0.6$, $\alpha = 45$ deg, and $x/d = 8$: a) w/U_∞ vs y/d; b) u/U_∞ vs y/d.

Figure 10 shows the measured u and w velocity components (in body coordinates) for $M_\infty = 0.6$, $\alpha = 25$ deg, and $x/d = 8$. The w component of velocity (Fig. 10a) shows the body vortices to be positioned symmetrically with respect to the body. The characteristic downwash of the body vortices can be seen between the vortices ($y = 0$) and the upwash of the vortices is noted outboard of each vortex. The magnitude of the downwash between the vortices, however, is larger than that measured in incompressible flows.[3] This implies that either the vortices are of higher strength or they simply are closer together. Away from each vortex the measurements approach the freestream value in body coordinates; $w_\infty/U_\infty = \sin\alpha$ and $u_\infty/U_\infty = \cos\alpha$.

The u velocity variation across the wake (Fig. 10b) shows slight velocity excesses ($u/U_\infty > \cos\alpha$) and velocity defects ($u/U_\infty < \cos\alpha$), except for $z/d = 0.833$. For $z/d = 0.833$ the axial velocity excursions, both positive and negative, are roughly 50 m/s. It is believed that this is an experimental inaccuracy and not a flowfield characteristic. This excursion could be caused by a slight difference in the location of the focal volume of each component of the laser. The mismatch in focal volumes only produces a significant error in velocity when there is a very large gradient in velocity. A large velocity gradient occurs at both of the axial velocity excursions shown in Fig. 10b. A simple estimate can be made of the required mismatch to produce the 50 m/s magnitude. The LV data were obtained in wind tunnel coordinates¶ so that the transformation to body coordinates is $u = u'\cos\alpha - w'\sin\alpha$. The approximate value of $\partial u'/\partial y$ and $\partial w'/\partial y$ at the location of interest was calculated to be 28 (m/s)/mm. Then to produce an error of 50 m/s only requires a mismatch of 1.8 mm.

¶Note that if the velocity data are presented in wind tunnel coordinates, then no velocity deviation can be seen.

Figure 11 shows u and w velocity components for $M_\infty = 0.6$, $\alpha = 35$ deg, and $x/d = 8$. The variation of w across the wake shows that it is slightly asymmetric for this angle of attack. Comparing the measurements for $z/d = 0.916$ with the corresponding vapor screen (Fig. 5b) it is seen that this height above the body passes through the center of the right vortex. Although the left vortex is not visible, both the u and w variations for $z/d = 1.5$ suggests it is located slightly above the right vortex. Note that the u velocity excursion which occurred for $\alpha = 25$ deg does not occur for $\alpha = 35$ deg even though the gradients in u' and w' are roughly the same as at $\alpha = 25$ deg.

The u and w velocities for $M_\infty = 0.6$, $\alpha = 45$ deg, and $x/d = 8$ are shown in Fig. 12. For this angle of attack the lateral shift in vortex locations is evident in both the u and w plots. The y/d position of the minimum value of w moves from -0.267 for $z/d = 1.167$ to 0.433 for $z/d = 3.167$. Comparing this to the appropriate vapor screen photograph (Fig. 5c), it is seen that this is consistent with the leftward displacement of the vortex nearest the body and the rightward displacement of the next higher vortex. The u velocity distribution shows a similar shift in velocity excess and defect as one moves away from the body. The side force coefficient for laser velocimeter data obtained at $\alpha = 35$ and 45 deg was 0.86 and -0.35, respectively. These were the same side force values that were measured when the laser vapor screen photographs were obtained for $\alpha = 35$ and 45 deg, respectively, for $x/d = 8$.

IV. Conclusions

The capabilities of a new dual beam, forward scatter, laser velocimeter for the NASA Ames 1.83×1.83 m wind tunnel have been demonstrated. The present measurements obtained at three different body stations and three angles of attack represent the first LV data of the compressible body vortex

wake at high Reynolds number. A simple modification to the LV sending optics has demonstrated that high resolution laser vapor screen flow visualization can be achieved in both subsonic and supersonic flow. This capability can be effectively used prior to LV data acquisition to determine regions for detailed study, thus reducing wind tunnel test time. The side force data show that a wide range of values could exist on the body for the same angle of attack, Mach number, and roll angle. Three for four different values of side force for the same angle of attack were repeated consistently over a period of three weeks of wind tunnel testing. From this we conclude that multiple, metastable, asymmetric, vortex states can exist, at least for the test Reynolds number, on a body at the same roll angle even though no known flow parameters were changed. As it is now accepted that the asymmetric body vortex wake is sensitive to phenomena such as nosetip imperfections and roll angle, it is not unreasonable to find that the asymmetric wake is essentially unstable, that is, sensitive to the point that wind tunnel conditions cannot be perfectly repeated. In fact it is hypothesized that as the nosetip imperfection scale is decreased the asymmetric wake becomes more sensitive to other secondary disturbances because no body surface trip is provided. Consequently, it is recommended for future experiments that simultaneous velocity component measurements be made while continually monitoring either, or both, the surface pressure distribution or the side force on the body.

Acknowledgments

The authors would like to thank Dr. Donald C. Daniel, Aerodynamics Research Manager, Air Force Armament Laboratory and Dr. Gary T. Chapman, Senior Staff Scientist, NASA Ames Research Center, for their comments and suggestions during this investigation. This work was sponsored by the Air Force Armament Laboratory, Eglin AFB, Fla., under AF Contract F08635-77-C-0049 and by NASA under Contract NAS2-9663.

References

[1] Deffenbaugh, F. D. and Koerner, W. G., "Asymmetric Wake Development on Missiles at High Angles of Attack," *Journal of Spacecraft and Rockets*, Vol. 14, March 1977, pp. 155-162.

[2] Kruse, R. L., "Influence of Spin Rate on Side Force of an Axisymmetric Body," *AIAA Journal*, Vol. 16, April 1978, pp. 415-416.

[3] Fidler, J. E., Nielsen, J. N., and Schwind, R. G., "An Investigation of Slender-Body Wake Vortices," AIAA Paper 77-7, AIAA 15th Aerospace Sciences Meeting, Jan. 1977.

[4] Yanta, W. J. and Wardlaw, A. B., "Laser Doppler Velocimeter Measurements of Leeward Flowfields on Slender Bodies at Large Angle of Attack," AIAA Paper 77-660, AIAA 10th Fluid and Plasma Dynamics Conference, June 1977.

[5] Owen, F. K. and Johnson, D. A., "Wake Vortex Measurements of Bodies at High Angle of Attack," AIAA Paper 78-23, AIAA 16th Aerospace Sciences Meeting, Jan. 1978.

[6] Owen, F. K., "Transition Experiments on a Flat Plate at Subsonic and Supersonic Speeds," *AIAA Journal*, Vol. 8, March 1970, pp. 518-523.

[7] Lamont, P. J. and Hunt, B. L., "Pressure and Force Distribution on a Sharp-Nosed Circular Cylinder at Large Angles of Inclination in a Uniform Subsonic Stream," *Journal of Fluid Mechanics*, Vol. 76, Pt. 3, 1976, pp. 519-559.

[8] Hunt, B. L. and Dexter, P. C., "Pressures on a Slender Body at High Angle of Attack in a Very Low Turbulence Level Air Stream," *AGARD Conference Proceedings No. 247, Fluid Dynamics Panel Symposium*, Oct. 1978.